Local Structure of Semiflexible Polymer Melts†

Kevin G. Honnell,* John G. Curro, and Kenneth S. Schweizer

Sandia National Laboratories, Albuquerque, New Mexico 87185

Received November 16, 1989; Revised Manuscript Received February 1, 1990

ABSTRACT: Polymer RISM (reference interaction site model) theory is used to examine the intermolecular radial distribution function and isothermal compressibility of semiflexible polymer melts. Chains are modeled as a series of linked, hard sites with a local bending energy proportional to the cosine of the bond angle. Chain stiffness is controlled by a single parameter, the persistence length, which may be matched to the material of interest. Comparisons of the predicted intermolecular radial distribution functions to the molecular dynamics results of Grest and Kremer for chains of 50, 100, and 150 sites show very good agreement on all length scales. Parametric studies as a function of chain length and chain stiffness reveal that as the characteristic stiffness is increased beyond three bond lengths, the radial distribution function and isothermal compressibility saturate, becoming relatively insensitive to chain length or stiffness. At low densities the local structure is dominated by a correlation hole, indicating a relative absence of intermolecular neighbors, while at high densities the pair correlation function shows a peak and valley structure, qualitatively similar to that of monatomic fluids.

I. Introduction

A series of recent papers has charted the development of the first tractable, statistical-mechanical theory for the equilibrium structure of dense polymer melts.[1-7] The theory, which is based on an integral-equation approach, affords a first-principles look at the local and long-range structure, thermodynamic behavior, and phase stability of polymeric fluids, without resorting to the mean-field and lattice-based assumptions inherent in earlier models. In addition, predictions for structural properties, such as the static structure factor, can be compared to experimental results obtained through X-ray and neutron scattering. Previous applications have examined the site–site pair correlation function,[1-4] structure factor,[1,2,5] and equation of state[6] of model homopolymer melts, as well as the intermolecular structure, thermodynamic behavior, and apparent χ parameter of binary blends.[7] In this paper we explore the effects of chain stiffness on the intermolecular structure of homopolymer melts. An understanding of the role played by chain stiffness is essential for a quantitative theoretical description of the thermodynamics and phase behavior of polymer melts and blends.

Our approach is based on an interaction site model of polymer structure. Each chain is modeled as a series of spherically symmetric "sites" which interact through hard-sphere potentials. Structural correlations are described by using the RISM ("reference interaction site model") formalism, originally developed by Chandler and Andersen for small, rigid molecules[8] and extended to polymers by two of the present authors.[1-7] As applied to polymers, RISM theory describes the pair correlations between sites on neighboring chains, as summarized by the intermolecular site–site radial distribution function. In brief, given a knowledge of the intramolecular structure of a single chain, the theory describes the packing of chains in the melt and the consequent thermodynamic behavior.

Unfortunately, in the RISM theory for flexible polymers the intramolecular structure is coupled nonlinearly to the intermolecular structure, and, in general, cannot be predicted a priori.[3,4,9] For dense melts, though, the problem can be rendered tractable by invoking the Flory "ideality" postulate—namely, that the long-range intramolecular interactions in the melt are effectively screened out, down to nearly monomeric length scales, by intermolecular interactions.[10-12] In other words, a polymer chain in the melt has a configuration characteristic of a chain in a Θ solvent and (on length scales long compared to a segment length) exhibits random-flight scaling. This ideality has been predicted from theoretical arguments[10-12] and confirmed by experimental studies[13] and computer simulation.[14] Thus, to a first approximation, the intramolecular structure can be obtained from a single-chain calculation in which *long-range* repulsive and medium-induced interactions are ignored.

Previous numerical calculations have focused on Gaussian[1,3,5,7] and ideal freely jointed chain models.[3-5] These models invoke the ideality assumption on all length scales. Bond angles are random, so that the bond vectors between successive sites are completely uncorrelated. Though sufficient to describe the universal, long-wavelength properties of chains, these models were found incapable of capturing some important structural details on monomeric length scales. In particular, comparisons with recent molecular dynamics results for nonoverlapping, freely jointed chains revealed that the idealized models tend to underestimate the heights of the first and second peaks in the radial distribution function and that their intramolecular structure factors differed significantly from those observed in simulation.[4] By increasing the segmental bond length, however, much better agreement with simulation was obtained on short length scales (at the expense of shifting the secondary maxima and minima outward to unrealistic positions). This suggests that the main deficiency of these ideal models is their unrealistic flexibility on short length scales rather than their neglect of long-range excluded volume.

Accordingly, the object of this study is to implement a more realistic chain model capable of describing correlations on all length scales and potentially applicable to polymeric systems of practical interest. To this end, we have employed a discrete analogue of the "wormlike" chain[15,16] which retains the variable stiffness inherent in the original worm model while incorporating discrete sites along the chain backbone to mimic monomeric subunits. Use of a semiflexible model allows us to include approximately the *local* stiffness present in real chains due to molecular bonding constraints and bond rotational poten-

† Supported by the U.S. Department of Energy under Contract DE-AC046-DP00789.

0024-9297/90/2223-3496$02.50/0

tials, as well as the induced stiffness arising from incompletely screened excluded-volume interactions.

The wormlike chain, first introduced by Kratky and Porod[17] in 1949, has long served as a useful model in probing the effects of local chain stiffness and in interpreting the results of light-scattering and X-ray measurements on semiflexible chains.[15-20] In this model, the chain is regarded as a continuous space curve with a local energy density associated with bending. Local stiffness is controlled by a single parameter, the persistence length. Although the exact intramolecular pair correlation function is unknown for this model, Koyama[18] has given an accurate approximate expression which interpolates between the known flexible-coil and rigid-rod limits while reproducing the exact second and fourth moments of the distribution. However, because RISM is inherently a site–site approach, the continuous worm is not directly amenable to investigation.

In constructing a discrete-chain analogue of the worm, we replace the continuous curve by a series of linked, rigid rods in which the local bending energy is proportional to the cosine of the bond angle. By adjusting the persistence length, chain behavior can be varied from the flexible-coil to rigid-rod limits. The general functional form of the Koyama distribution is also applicable to this discrete model, thus supplying the required input into the RISM theory. Connection to experiment or computer simulation is made by matching a geometrical property of the semiflexible chain, such as the persistence length or average squared end-to-end distance, to the physically observed value.

Comparisons of theoretical calculations using the model described above with the recent molecular dynamics results of Grest and Kremer[4,21] for chains of 50–200 segments show very good agreement on all length scales. Parametric studies as a function of persistence length, density, and chain length reveal that as the characteristic stiffness (persistence length) is increased to three or four monomeric units, the radial distribution function and isothermal compressibility saturate, becoming relatively insensitive to chain length or persistence length. On short length scales, though, the local structure is extremely sensitive to changes in density.

Section II begins with a review of polymer RISM theory and a discussion of the semiflexible chain model. We then describe an approximate method for estimating the packing fraction of the model fluid and outline a perturbative scheme which allows predictions for hard-core fluids to be related to systems with soft-core repulsions. Numerical results are presented in section III, beginning with comparisons to molecular dynamics results and continuing with parametric studies as a function of chain length and stiffness. Finally, section IV concludes with some brief remarks and an overview of key results.

II. Theory

A. Polymer RISM Theory. The principal result of polymer RISM theory is a description of the local site density in the fluid, as measured by the site–site intermolecular radial distribution function, $g(r)$. This distribution function is proportional to the probability of finding two sites on *different* chains separated by a distance r. A value of $g(r) > 1$ implies that the local density is greater than the average density, while a value of $g(r) < 1$ indicates that it is less.

The starting point for the theory is the generalized Ornstein–Zernike matrix equation developed by Chandler and Andersen.[8] This equation expresses the correlations between two *specific* sites α and γ on different chains in terms of a "direct" component, propagated directly between the two molecules, and an "indirect" component, mediated through a third molecule. For a chain composed of N identical sites, the generalized Ornstein–Zernike description results in $N(N+2)/8$ coupled, nonlinear integral equations corresponding to all distinct (α,γ) combinations [$(N+1)(N+3)/8$ equations if N is odd], making the problem seemingly intractable for high polymers. However, for a chain-averaged description of the local structure and radiation scattering, as well as an evaluation of thermodynamic properties such as the bulk compressibility and equation of state, the quantity of key interest is the mean correlation function $g(r)$, obtained by averaging over all (α,γ) pairs. A perturbative analysis shows that for this quantity the system of coupled integral equations reduces to a single nonlinear integral equation[2]

$$h(r) = \int d\mathbf{r}' \int d\mathbf{r}'' \, \omega(|\mathbf{r} - \mathbf{r}'|) c(|\mathbf{r}' - \mathbf{r}''|)[\omega(r'') + \rho_m h(r'')] \tag{1}$$

with the corrections being of $O(1/N^2)$. Here, ρ_m is the average monomer (or site) density, $h(r) \equiv g(r) - 1$ is the total correlation function, and $\omega(r)$ is the single-chain correlation function

$$\omega(r) = \frac{1}{N}\sum_{\alpha,\gamma} \omega_{\alpha\gamma}(r) \tag{2}$$

where $\omega_{\alpha\gamma}(r)$ is the probability density of finding sites α and γ on the same chain separated by a distance r. $c(r)$ is the direct correlation function, which can be considered as being defined through eq 1. Physically, eq 1 follows from the neglect of *explicit* chain-end effects on the intermolecular correlations, though such end effects are incorporated implicitly through $\omega(r)$. In Fourier-transform space, eq 1 becomes simply

$$\hat{h}(k) = \hat{\omega}(k)\hat{c}(k)[\hat{\omega}(k) + \rho_m \hat{h}(k)] \tag{3}$$

Generalization of eq 3 to polymer chains composed of nonidentical sites is straightforward.

To uniquely determine $h(r)$ and $c(r)$, the Percus–Yevick closure relations are introduced[8,22]

$$h(r) = -1 \qquad r < \sigma \tag{4}$$

$$c(r) = 0 \qquad r > \sigma \tag{5}$$

where σ is the hard-sphere diameter of a site. Equation 4 is an exact relation which reflects the impenetrability of the hard spheres, while eq 5 is an approximation which follows from a literal interpretation of the "direct" nature of $c(r)$. Equation 1 together with these closure relations defines the polymer RISM theory.

Equation 1 is solved by using the variational approach of Lowden and Chandler.[23] In analogy with the exact (Percus–Yevick) solution for $N = 1$,[22] the direct correlation function is assumed to be a cubic polynomial in r

$$c(r) = H(\sigma - r)\sum_{i=1}^{4} a_i \left(\frac{r-\sigma}{\sigma}\right)^{i-1} \tag{6}$$

which identically satisfies eq 5. Here, $H(x)$ denotes the Heaviside step function. The a_i are unknown coefficients to be determined subject to the two remaining conditions, eqs 1 and 4. Equations 1 and 4 are satisfied by the functional relation

$$\frac{\delta I_{\mathrm{RISM}}}{\delta c(r)} = 0 \qquad r < \sigma \tag{7}$$

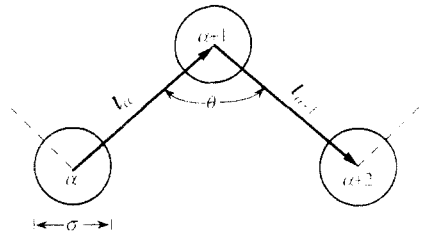

Figure 1. Local chain geometry. The bending energy is directly proportional to 1 + cos θ.

where

$$I_{\mathrm{RISM}} \equiv \rho_m^2 \int c(r)\, d\mathbf{r} - \frac{1}{8\pi^3}\int d\mathbf{k}\, \{\rho_m \hat{\omega}(k)\hat{c}(k) + \ln [1 - \rho_m \hat{\omega}(k)\hat{c}(k)]\} \quad (8)$$

Substitution of eqs 6 and 8 into eq 7 leads to four coupled nonlinear *algebraic* equations for the a_i, which are solved by standard numerical techniques. $h(r)$ is then determined through Fourier inversion of eq 3.

B. Intramolecular Structure Factor for a Semiflexible Chain. The only piece of information missing from the above analysis is an expression for the intramolecular structure factor, $\hat{\omega}(k)$, required in eq 8. The semiflexible model considered here is constructed as a discrete analogue of the wormlike chain. In the worm model, the chain is viewed as a continuous space curve with an elastic bending energy. Chain stiffness is controlled by a single, energy parameter, ϵ. If $\mathbf{u}(s)$ is the unit tangent to the curve at the point s, then the local energy density is given by[16,19]

$$E(s) = \frac{1}{2}\epsilon \left| \frac{d\mathbf{u}}{ds} \right|^2 \quad (9)$$

The total energy of the worm is then found by integrating $E(s)$ over all s.

In passing to a discrete representation of a semiflexible chain, the continuous curve is replaced by a series of $N - 1$ linked rods of length l, and the derivative of the unit tangent with respect to contour length is replaced by its discrete counterpart, $(\mathbf{l}_{\alpha+1} - \mathbf{l}_\alpha)/l$, where $\mathbf{l}_\alpha$ is the bond vector between sites α and $\alpha + 1$. (See Figure 1.) In analogy with eq 9, the bending energy associated with sites α, $\alpha + 1$, and $\alpha + 2$ is then given by

$$E_\alpha = \frac{1}{2l^2}\epsilon(\mathbf{l}_{\alpha+1} - \mathbf{l}_\alpha)\cdot(\mathbf{l}_{\alpha+1} - \mathbf{l}_\alpha) = \epsilon(1 + \cos\theta) \quad (10)$$

where θ is the bond angle formed by the three sites. In keeping with the ideality postulate, we neglect long-range intramolecular interactions, so the total energy of the chain is simply given by a sum over all of the bond angles.

Additional realism can be introduced into the stiff-chain model by including the short-range excluded-volume interactions between sites separated by two bonds. In the linked hard-sphere model, this restricts the allowable values of θ to $\theta \geq \theta_0$, where

$$\cos\theta_0 = 1 - \frac{\sigma^2}{2l^2} \quad (11)$$

Alternatively, if one views each site as representing a collection of actual monomeric units (e.g., a statistical chain segment), it may be appropriate to allow for some degree of site–site interpenetration. Here, we adopt the impenetrable viewpoint, in order to make contact with computer simulation results.

The exact intramolecular distribution functions for these semiflexible models are unknown. For the worm, however, Koyama has given an accurate approximate expression which interpolates between rigid-rod and Gaussian-coil limits while reproducing (by construction) the correct second and fourth moments of the distribution:[18,20]

$$\omega_{\alpha\gamma}(r) = \frac{1}{8\pi^{3/2}ABr}[e^{-(r-B)^2/(4A^2)} - e^{-(r+B)^2/(4A^2)}] \quad (12)$$

where

$$A^2 = \langle r_{\alpha\gamma}^2\rangle(1 - C)/6 \quad (13)$$

$$B^2 = C\langle r_{\alpha\gamma}^2\rangle \quad (14)$$

$$C^2 = \frac{1}{2}\left(5 - 3\frac{\langle r_{\alpha\gamma}^4\rangle}{\langle r_{\alpha\gamma}^2\rangle^2}\right) \quad (15)$$

and α and γ are two points along the curve; $\langle r_{\alpha\gamma}^2\rangle$ and $\langle r_{\alpha\gamma}^4\rangle$ denote the second and fourth moments of the distribution between the two points. The Fourier transform of the distribution is given by

$$\hat{\omega}_{\alpha\gamma}(k) = \frac{\sin(Bk)}{Bk}e^{-A^2k^2} \quad (16)$$

As noted by Mansfield,[20] the Koyama distribution is not limited to wormlike chains but, rather, can be applied to any semiflexible model for which $\langle r_{\alpha\gamma}^2\rangle$ and $\langle r_{\alpha\gamma}^4\rangle$ are known (provided that $\langle r_{\alpha\gamma}^4\rangle/\langle r_{\alpha\gamma}^2\rangle^2 \leq 5/3$). For the model considered here, $\langle r_{\alpha\gamma}^2\rangle$ depends only on $\langle\cos\theta\rangle$ and, as a result, takes the same form as for the freely rotating chain[16]

$$\langle r_{\alpha\gamma}^2\rangle = nl^2\left[\frac{1 - \langle\cos\theta\rangle}{1 + \langle\cos\theta\rangle} + \frac{2\langle\cos\theta\rangle}{n}\frac{1 - (-\langle\cos\theta\rangle)^n}{(1 + \langle\cos\theta\rangle)^2}\right] \quad (17)$$

Here, $n \equiv |\alpha - \gamma|$ denotes the number of links between sites α and γ. The fourth moment is a function of both $\langle\cos\theta\rangle$ and $\langle\cos^2\theta\rangle$ and, hence, differs from that of the freely rotating chain. Porod has considered the calculation of $\langle r_{\alpha\gamma}^4\rangle$ for an arbitrary chain model with specified values of $\langle\cos\theta\rangle$ and $\langle\cos^2\theta\rangle$.[24] His final result, however, contains several algebraic errors; the correct result is as follows:

$$\langle r_{\alpha\gamma}^4\rangle = \langle r_{\alpha\gamma}^2\rangle^2 + D_{\alpha\gamma}l^4 \quad (18)$$

$$\frac{3}{2}D_{\alpha\gamma} = n^2\left(\frac{1+q}{1-q}\right)^2 - n\left\{1 + \frac{2q}{(1-q)^3}(6 + 5q + 3q^2) - \left(\frac{1+q}{1-q}\right)^2\frac{4p}{1-p}\right\} + \left\{\frac{2q}{(1-q)^4}(4 + 11q + 12q^2) - \frac{4p}{1-p}\left[1 + \frac{8q}{(1-q)^3} + \left(\frac{1+q}{1-q}\right)^2\frac{p}{1-p}\right]\right\} - q^n\frac{8q}{(1-q)^3}\left\{n(1 + 3q) + \frac{1 + 2q + 3q^2}{1-q} - \frac{2p}{(q-p)^2}[n(1-q)(q-p) + 2q^2 - pq - p]\right\} - \frac{6q^{2n+2}}{(1-q)^4} + p^n\left\{\frac{4}{1-p}\left[1 + \frac{8q}{(1-q)^3} - \left(\frac{1+q}{1-q}\right)^2\left(1 - \frac{p}{1-p}\right)\right] - \frac{16q^2}{(1-q)^3}\frac{1}{(q-p)^2}[q + q^2 - 2p]\right\} \quad (19)$$

$$q = -\langle\cos\theta\rangle \quad (20)$$

$$p = (3\langle\cos^2\theta\rangle - 1)/2 \quad (21)$$

$$n = |\alpha - \gamma| \quad (22)$$

All that remains, then, is to supply values for $\langle\cos\theta\rangle$ and $\langle\cos^2\theta\rangle$. Using eq 10, one may determine $\langle\cos\theta\rangle$ from an ensemble average over the allowable bond angles

$$\langle \cos\theta \rangle = \frac{\int_{\theta_0}^{\pi} e^{-\epsilon(1+\cos\theta)/k_BT} \cos\theta \sin\theta \, d\theta}{\int_{\theta_0}^{\pi} e^{-\epsilon(1+\cos\theta)/k_BT} \sin\theta \, d\theta} = \frac{1}{\epsilon^*} - \frac{e^{\epsilon^*} + \cos\theta_0 e^{-\epsilon^* \cos\theta_0}}{e^{\epsilon^*} - e^{-\epsilon^* \cos\theta_0}} \quad (23)$$

where k_BT denotes the product of Boltzmann's constant and the temperature, $\epsilon^* \equiv \epsilon/k_BT$ is a dimensionless energy parameter, and θ_0 is determined by the short-range excluded-volume interaction (eq 11). Similarly, $\langle \cos^2\theta \rangle$ is found to be

$$\langle \cos^2\theta \rangle = \frac{2}{\epsilon^*}\langle \cos\theta \rangle + \frac{e^{\epsilon^*} - \cos^2\theta_0 e^{-\epsilon^* \cos\theta_0}}{e^{\epsilon^*} - e^{-\epsilon^* \cos\theta_0}} \quad (24)$$

Thus, the intramolecular distribution is completely characterized by two parameters, N and ϵ^*. In place of ϵ^*, however, it is convenient to quantify chain stiffness in terms of the persistence length, ξ_p. The persistence length is a measure of the distance over which orientational correlations between bond vectors along the chain decay. Specifically, ξ_p is defined as[15,16]

$$\xi_p \equiv \lim_{N\to\infty} \frac{1}{l} \sum_{i=1}^{N-1} \mathbf{l}_1 \cdot \mathbf{l}_i \quad (25)$$

For the semiflexible chain, the inner products required by eq 25 depend only on $\langle \cos\theta \rangle$, so that ξ_p takes the same form as for the freely rotating chain[15,16]

$$\xi_p = \frac{l}{1 + \langle \cos\theta \rangle} \quad (26)$$

To implement this semiflexible model in RISM calculations, the first step is to choose values for N and ξ_p. Connection to experiment or simulation can be made by matching ξ_p to the physically observed value for the material of interest. This uniquely determines $\langle \cos\theta \rangle$ through eq 26 and, in turn, fixes ϵ^* and $\langle \cos^2\theta \rangle$ through eqs 23 and 24. For each distinct $|\alpha - \gamma|$, $\langle r_{\alpha\gamma}^2 \rangle$ and $\langle r_{\alpha\gamma}^4 \rangle$ are found through eqs 17–22 and substituted into the Koyama formula (eqs 13–16) to give $\hat{\omega}_{\alpha\gamma}(k)$. The intramolecular structure factor, $\hat{\omega}(k)$, is then found by numerically summing over all (α,γ) pairs (eq 2).

C. Overlap Correction. One unphysical aspect of the stiff-chain model which must be addressed stems from the presence of overlaps between nonbonded sites on the same chain, which decreases the amount of space occupied by the molecules. In comparing predictions for hard-core systems, it is desirable to carry out the comparison at constant packing fraction, so that the molecules in each system physically occupy the same amount of space. However, due to the neglect of intramolecular excluded-volume interactions, at a given packing fraction η the monomer density (ρ_m) of the ideal system considered here will be greater than the monomer density of the corresponding physical system. For a given η, the monomer density of our model system is given by

$$\rho_m = \frac{6\eta}{\pi\sigma^3} \frac{1}{1 - \Delta_N} \quad (27)$$

where Δ_N represents that fraction of the nominal chain volume ($N\pi\sigma^3/6$) which can be attributed to unphysical overlaps between nonbonded sites. Assuming pairwise overlaps, Δ_N may be estimated from[3]

$$\Delta_N \cong \frac{\int_0^{\sigma} \left[\frac{\pi\sigma^3}{6}\left(1 - \frac{3r}{2\sigma} + \frac{r^3}{2\sigma^3}\right)\right]\left(\sum_{\alpha,\gamma>\alpha+1} \omega_{\alpha\gamma}(r)\right)(4\pi r^2)\, dr}{N\pi\sigma^3/6} \quad (28)$$

The term enclosed in brackets in eq 28 is the overlap volume of two spheres of diameter σ whose centers are separated by a distance r, and the sums run over all nonbonded pairs.

As one would expect, the size of the overlap correction increases with chain length and decreases with chain stiffness. For a tangent hard-sphere model ($\sigma = l$) with $\xi_p = l$ and $\theta_0 = \pi/3$, Δ_N ranges from 0.043 when $N = 20$ to 0.135 when $N = 2000$. It is interesting to note that these values are considerably smaller than those required for Gaussian and freely jointed chains with the same persistence length.[3] For the tangent hard-sphere chain with $\xi_p = 3l$, Δ_N is reduced to 0.00015 when $N = 20$ and to 0.005 when $N = 2000$, so that the overlap correction is essentially negligible. As a result of the pair approximation used in formulating eq 27 (which overestimates the volume occupied by three or more overlapping sites), these estimates represent upper bounds on the true size of the correction.[3]

D. Soft-Core Potentials. Grest and Kremer have recently performed molecular dynamics simulations on dense systems of chains ranging from 10 to 400 monomeric units.[4,21] Given the general paucity of simulation data for off-lattice polymer melts, these calculations represent valuable benchmarks for assessing the accuracy of approximate theoretical models. The molecular model they examined, however, differs slightly from the hard-chain model considered here. In particular, bonds were allowed to vibrate within a stiff FENE (finite extensible nonlinear elastic) potential well, and, in place of the hard-sphere potential, nonbonded interactions were governed by a shifted, repulsive, Lennard-Jones potential

$$\frac{U_{LJ}(r)}{kT} = 4\left[\left(\frac{\sigma_{LJ}}{r}\right)^{12} - \left(\frac{\sigma_{LJ}}{r}\right)^{6} + \frac{1}{4}\right] H(2^{1/6}\sigma_{LJ} - r) \quad (29)$$

which vanishes at $r = 2^{1/6}\sigma_{LJ}$ in such a way that the potential energy and force remain continuous. Here, σ_{LJ} refers to the Lennard-Jones site diameter (as distinct from the hard-site diameter σ).

To meaningfully compare the RISM predictions to the simulation results, an accounting must be made for the differences in their respective chain models. In the simulations, the average squared bond length was observed to be $\langle l^2 \rangle = 0.94\sigma_{LJ}^2$, and bond-length fluctuations were very small by construction of the FENE potential. Accordingly, in the RISM calculations we employ a fixed bond length of $l = 0.94^{1/2}\sigma_{LJ}$. To account for the soft core of the repulsive Lennard-Jones potential, we use the highly accurate, perturbative method developed by Andersen, Weeks, and Chandler,[25] as discussed in ref 4. In brief, a state-dependent, effective hard-sphere diameter is chosen in order to minimize the difference between the Helmholtz free energies of the repulsive Lennard-Jones and hard-chain fluids. This is accomplished by annulling the first-order term in an expansion of the free energy of the repulsive Lennard-Jones system about a hard-chain reference fluid. Within the framework of polymer RISM theory, the optimum hard-sphere diameter is then given

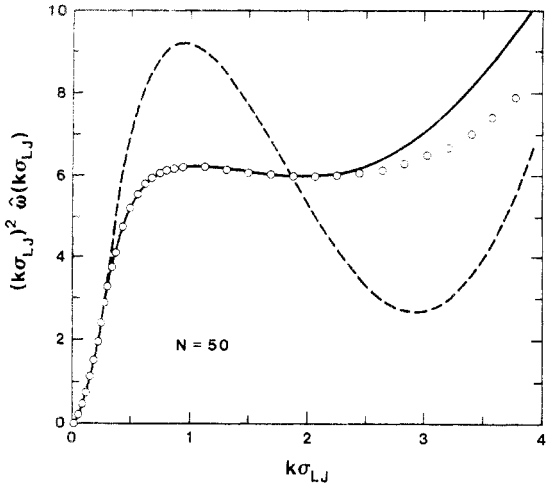

Figure 2. Comparison of theoretical and simulation results for the intramolecular structure factor of 50-mers, plotted in standard Kratky form. Points are the molecular dynamics results of Grest and Kremer.[4] The solid curve represents the semiflexible chain; the dashed curve corresponds to the nonoverlapping freely jointed chain of ref 4. Wave vectors are scaled with the Lennard-Jones site diameter.

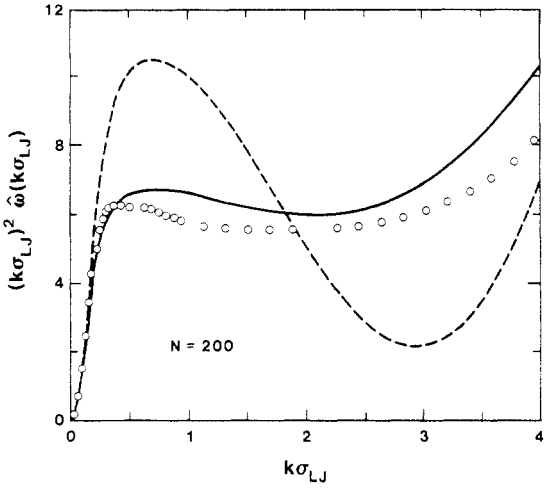

Figure 3. Comparison of theoretical and simulation results for the intramolecular structure factor of 200-mers, plotted in standard Kratky form. Points are the molecular dynamics results of Grest and Kremer.[4] The solid curve represents the semiflexible chain; the dashed curve corresponds to the nonoverlapping freely jointed chain of ref 4. Wave vectors are scaled with the Lennard-Jones site diameter.

by[4]

$$\int_0^{\sigma} c_{HS}(r)e^{-U_{LJ}(r)/k_BT}r^2\,dr + \int_{\sigma}^{2^{1/6}\sigma_{LJ}} g_{HS}(r)(1 - e^{-U_{LJ}(r)/k_BT})r^2\,dr = 0 \quad (30)$$

In practice, the effective σ is determined numerically, using an iterative, trial-and-error procedure. An initial guess for σ is made, and the RISM equations are solved for $c_{HS}(r)$ and $g_{HS}(r)$. The left-hand side of eq 30 is then evaluated and used to construct the next estimate for σ. This process is repeated until eq 30 is satisfied to within a specified tolerance—in the present case, 10^{-6}. Generally, five to eight iterations are sufficient for convergence. Note that on each iteration, the size of the overlap correction given by eqs 27 and 28 changes slightly due to the adjusted σ. For chains of 50–200 sites, the ratio of σ/σ_{LJ} ranged from 1.0145 to 1.0148. These values are very similar to those previously obtained for freely jointed chain models.[4]

Within the context of the Anderson–Weeks–Chandler perturbation theory, the radial distribution function for the soft-core fluid is then given by[4,25]

$$\begin{aligned} g_{LJ}(r) &\cong -c_{HS}(r)e^{-U_{LJ}(r)/k_BT} \qquad r \le \sigma \\ &\cong g_{HS}(r)e^{-U_{LJ}(r)/k_BT} \qquad \sigma \le r \le 2^{1/6}\sigma_{LJ} \\ &\cong g_{HS}(r) \qquad r \ge 2^{1/6}\sigma_{LJ} \end{aligned} \quad (31)$$

This correction decreases the peak at contact by roughly 20%, relative to $g_{HS}(r)$, and shifts it outward to the vicinity of 1.07σ.

III. Numerical Results

A. Comparison with Simulation. Predictions for the intramolecular structure factor of the semiflexible chain (SFC) are plotted in standard Krakty form in Figures 2 ($N = 50$) and 3 ($N = 200$) along with the molecular dynamics (MD) results of Grest and Kremer.[4,21] Simulations were performed at a site density $\rho_m\sigma_{LJ}^3 = 0.85$. Also shown in Figure 2 are the predictions for the nonoverlapping freely jointed chain (NFJC) discussed previously in ref 4. In the NFJC model, the chain segments are freely jointed, but unphysical overlaps between nonbonded segments are explicitly removed from the intramolecular distribution function.[3]

In each plot, the persistence length of the SFC was determined by matching the average squared end-to-end distance to the random-walk scaling form observed in the simulations[4,21]

$$\langle R^2 \rangle = 1.80N\langle l^2 \rangle \quad (32)$$

In this way, ξ_p/l was found to range from 1.43 for $N = 50$ to 1.41 for $N = 200$. It is interesting to note that these values are only slightly larger than the value 1.38 obtained by neglecting all excluded-volume interactions save the short-range interaction given by eq 11 (i.e., setting $\epsilon = 0$ in eqs 10, 23, and 24). This reinforces the notion that, in dense melts, chain expansion is primarily a local phenomenon which can be accurately represented by ideal models of the type considered here. (Incidentally, the persistence lengths given above correspond to a freely rotating chain with fixed bond angles in the neighborhood of 107°—quite close to the tetrahedral angles present in *n*-alkanes.)

The general shape of the SFC and MD Krakty plots in Figures 2 and 3 can be broken into three distinct regions:[24] a Gaussian branch at small k characterizing the global dimensions of the chain; a transition region, where $\hat{\omega}(k) \propto k^{-2}$; and an outer branch where $\hat{\omega}(k) \sim 1$. Both the SFC and NFJC models give good agreement with simulation in the Gaussian regime, confirming the usefulness of idealized models in describing the long-wavelength properties of real chains. Similarly, for large wave vectors, where $\hat{\omega}(k)$ is dominated by self- and rigid-bond correlations, one expects good agreement between the various models (simulation results extend only to $k\sigma_{LJ} \approx 4$). However, in the intermediate, plateau region, the SFC offers substantial improvement over the NFJC predictions.

This intermediate scaling regime, $R_g^{-1} \lesssim k \lesssim l^{-1}$, is of particular importance, as it characterizes local chain stiffness. One can gain some qualitative insight into the location and shape of this transition region by considering the behavior of a single ideal chain.[4] In the intermediate wave vector regime, the intramolecular structure factor is expected to scale as[26]

$$k^2\hat{\omega}(k) \cong 12N/\langle R^2 \rangle \quad (33)$$

For long chains, $\langle R^2 \rangle \sim Nl(2\xi_p - l)$ (see eqs 17 and 26),

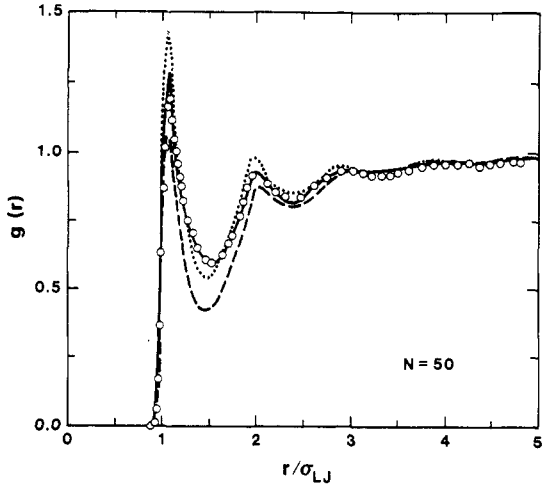

Figure 4. Intermolecular radial distribution function for soft-core 50-mers at $\eta = 0.463$. Points are the simulation results of Grest and Kremer[4] (some points are omitted for clarity). Curves are the predictions of polymer RISM theory using the semiflexible model (solid), the nonoverlapping freely jointed model (dashed), and the simulated $\hat{\omega}(k)$ displayed in Figure 2 (dotted). Distances are scaled by the Lennard-Jones site diameter.

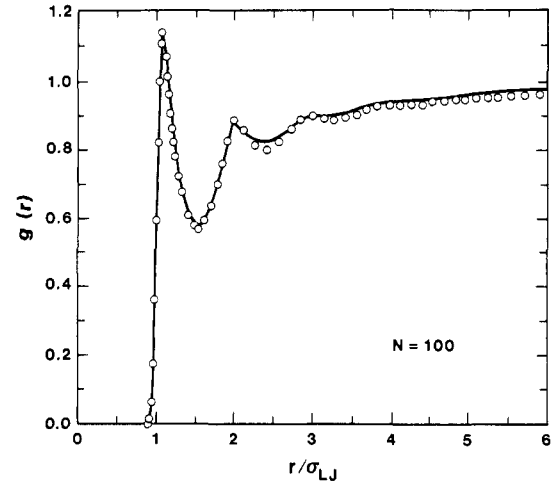

Figure 5. Intermolecular radial distribution function for soft-core 100-mers at $\eta = 0.464$. Points are the simulation results of Grest and Kremer[21] (some points are omitted for clarity); the curve denotes the predictions of the semiflexible model. Distances are scaled by the Lennard-Jones site diameter.

so that

$$k^2\hat{\omega}(k) \cong 12/[l(2\xi_p - l)] \tag{34}$$

The height of the plateau is thus a decreasing function of the persistence length. For Gaussian and freely jointed models, where $\xi_p = l$, one expects the plateau to occur at $(k\sigma^2)\hat{\omega}(k) \approx 12(\sigma/l)^2$ (or, for finite length chains, at slightly smaller values); the loop in the nonoverlapping freely jointed curve in Figures 2 and 3 is caused by the explicit removal of intramolecular site–site overlaps from $\omega(r)$, which induces some stiffness in the model. For the SFC, this approximate calculation places the plateau in the neighborhood of 6.5–7, in line with the results shown in Figures 2 and 3.

Overall, the SFC model appears to give a fairly accurate representation of the intramolecular structure factor, particularly for $N = 50$. For $N = 200$, the agreement drops off slightly (although statistics from the simulations suggest that the $N = 200$ MD results may be somewhat less reliable[27]). Both the $N = 50$ and $N = 200$ theoretical curves deviate from the MD results, however, in the transition from plateau to large-k behavior, $3 < k\sigma_{LJ} < 6$. This may be due to some residual nonphysical overlap between neighboring nonbonded sites separated by two or three bonds. Although eq 11 was intended to explicitly remove overlaps between sites separated by two bonds, the Koyama distribution is only an approximate representation, based on ideal moments, of the true $\omega(r)$ and, as such, allows for some residual overlap between second neighbors. Since the structure factor in this regime is extremely sensitive to correlations over distances of order l, unrealistic short-ranged overlaps could be a source of error in $\omega(r)$. Along these lines, we found that if the calculations were repeated with the same values for ξ_p but with $\theta_0 = 0$ (so that the stiffness remained constant, but overlaps were not otherwise discouraged [eqs 11, 23, and 24]), the SFC curves shifted farther away (upward) from the MD results and that the transition from plateau to rigid-rod domains became less distinct.

In Figures 4–6, RISM predictions for the intermolecular radial distribution function, $g(r)$, of the SFC are compared to simulation results for $N = 50$, 100, and 150. Also shown in Figure 4 are the NFJC and "exact" predictions, discussed previously in ref 4. The "exact" results were

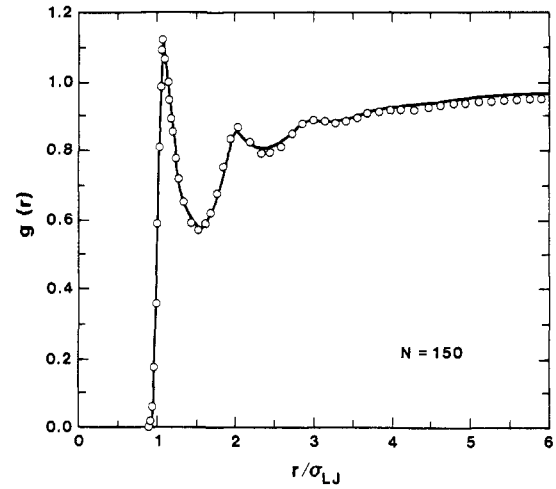

Figure 6. Intermolecular radial distribution function for soft-core 150-mers at $\eta = 0.464$. Points are the simulation results of Grest and Kremer[21] (some points are omitted for clarity); the curve denotes the predictions of the semiflexible model. Distances are scaled by the Lennard-Jones site diameter.

obtained by substituting the simulated $\hat{\omega}(k)$ (plotted in Figure 2) into the polymer RISM formalism. On short length scales, the local structure is seen to be "liquid-like", displaying shells of first- and second-nearest neighbors. Over longer distances, though, the curves exhibit a spatially slowly varying "correlation hole", corresponding to relative absence of neighboring sites due to intramolecular screening.[3,28]

Overall, the agreement between the SFC and MD predictions is quite good on all length scales, a slight tendency to underestimate the depths of the second and third valleys notwithstanding. The improvement over the "exact" results at contact, however, must be regarded as fortuitous. (Indeed, RISM, as well as its precursor, the Percus–Yevick theory, is known to be less reliable near contact.[29]) The NFJC predictions are in qualitative agreement with simulation at small r, becoming more accurate as the distance is increased. This is a reflection of the accuracy of the NFJC in the relatively small-k (large-r) regime and of its shortcomings in the intermediate scaling regime. Indeed, given the differences between the simulated and NFJC $\hat{\omega}(k)$ for $k\sigma_{LJ} > 1$, the overall agreement between their $g(r)$ is quite remarkable. This highlights the utility of coarse-grained descriptions in describ-

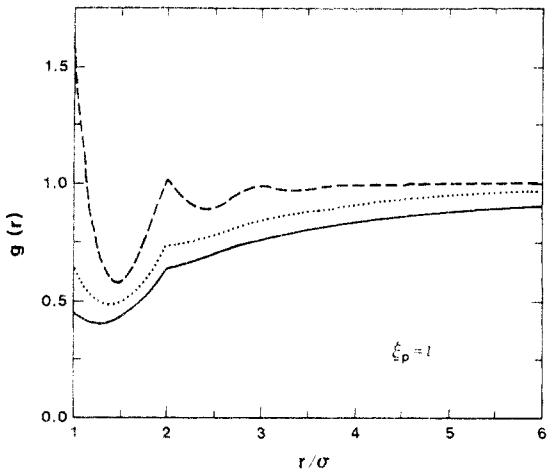

Figure 7. Intermolecular radial distribution function for tangent hard-sphere chains at a fixed persistence length, $\xi_p = l$, and three degrees of polymerization: $N = 20$ (dashed), 200 (dotted), and 2000 (solid). Distances are scaled by the hard-site diameter; the total monomer packing fraction is $\eta = 0.5$. For $N = 20$, $g(\sigma) \approx 1.65$; for $N = 200$, $g(\sigma) \approx 0.67$; and for $N = 2000$, $g(\sigma) \approx 0.46$.

ing correlations on longer length scales and, at the same time, underscores the need to have an accurate representation of local stiffness in the intermediate scaling regime to predict short-range structure.

As the chain length is increased (Figures 5 and 6), the height of the first peak in the SFC predictions drops off slightly relative to the molecular dynamics results, which appear remarkably insensitive to chain length. The overall agreement, however, remains very good. This decrease in the contact value relative to the simulation results may be due to the greater likelihood of intramolecular overlap for the longer chains, which can more easily bend back and self-intersect, increasing reliance on the approximate overlap correction described in section II.C. Along these lines, we repeated the calculations setting $\Delta_N = 0$ in eq 27, so that the overlap correction was omitted. As expected, this resulted in a damping of the short-range structure, decreasing the height of the first peak by ca. 5–6% and the depth of the first valley by roughly 1%. A much larger effect was obtained by holding the stiffness of the chains fixed (i.e., ξ_p) while setting $\epsilon^* = 0$ in eqs 23 and 24, so that overlaps between sites separated by two bonds were no longer actively suppressed. This produced a larger damping effect, decreasing the height of the first peak by 12–14% and the depth of the first valley by ca. 5%. Apparently, an accurate representation of intramolecular correlations over distances of two to three bond lengths is the key to obtaining quantitatively reliable predictions for the local structure.

B. Parametric Studies. Having demonstrated the accuracy of polymer RISM theory, we now turn to an examination of the effects of chain stiffness and chain length on the local structure of melts. Figures 7–10 show a series of plots, each at a fixed persistence length, of $g(r)$ vs r for chain lengths ranging from 20 to 2000. These calculations were performed on a tangent hard-sphere model ($\sigma/l = 1$) at a packing fraction $\eta = 0.5$.

Figure 7 displays results for flexible chains ($\xi_p = l$) of lengths $N = 20$, 200, and 2000. The short-range structure for these flexible chains is seen to be a strong function of N. In the high-polymer fluid ($N = 2000$) the local density is depleted relative to the bulk, while in the short-chain fluid ($N = 20$), it is enhanced. This behavior may be attributed to the high degree of intramolecular flexibility, which is conducive to the formation of relatively compact coils. For example, in the $N = 2000$ case, an individual site is likely to find itself embedded in a sea of intramolecular neighbors which effectively exclude sites

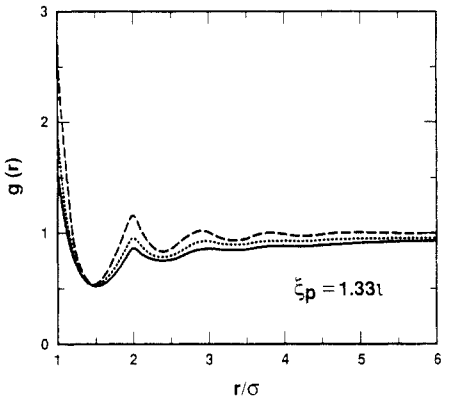

Figure 8. Intermolecular radial distribution function for tangent hard-sphere chains at a fixed persistence length, $\xi_p = 1.33l$, and three degrees of polymerization: $N = 20$ (dashed), 200 (dotted), and 2000 (solid). Distances are scaled by the hard-site diameter; $\eta = 0.5$. For $N = 20$, $g(\sigma) \approx 2.66$; for $N = 200$, $g(\sigma) \approx 1.84$; and for $N = 2000$, $g(\sigma) \approx 1.56$.

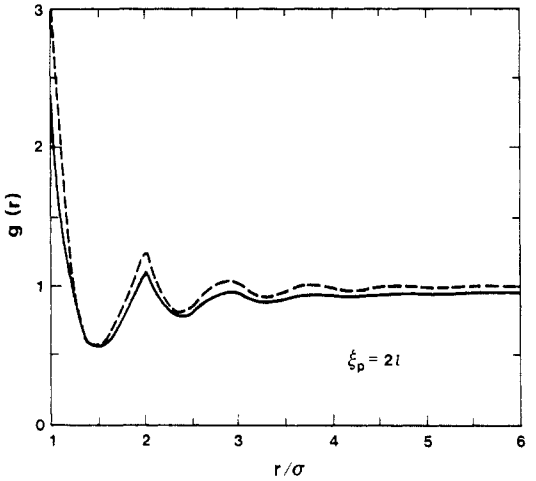

Figure 9. Intermolecular radial distribution function for tangent hard-sphere chains at a fixed persistence length, $\xi_p = 2l$, and two degrees of polymerization: $N = 20$ (dashed) and 2000 (solid). Distances are scaled by the hard-site diameter; $\eta = 0.5$. For $N = 20$, $g(\sigma) \approx 3.18$; for $N = 2000$, $g(\sigma) \approx 2.61$.

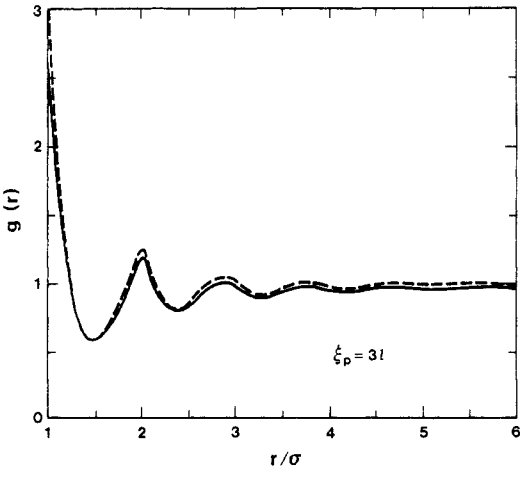

Figure 10. Intermolecular radial distribution function for tangent hard-sphere chains at a fixed persistence length, $\xi_p = 3l$, and two degrees of polymerization: $N = 20$ (dashed) and 2000 (solid). Distances are scaled by the hard-site diameter; $\eta = 0.5$. For $N = 20$, $g(\sigma) \approx 3.23$; for $N = 2000$, $g(\sigma) \approx 2.96$. Results for $\xi_p = 5l$ are nearly identical with those shown here.

on other chains from the neighboring vicinity. This intramolecular screening gives rise to the correlation hole in the intermolecular radial distribution function, reflecting the relative absence of intermolecular neighbors. As the chain length is decreased, the shielding effect diminishes and $g(r)$ shifts upward, so that by $N = 20$ there is a relative enhancement of sites near contact ($r = \sigma$), though a shallow correlation hole persists out to $r \approx 3\sigma$.

As chain stiffness is increased, there is a dramatic change in the local structure (Figures 8–10). Figure 8 shows results for $N = 20$, 200, and 2000 at $\xi_p = (4/3)l$. This is the persistence length obtained by setting $\epsilon^* = 0$ in eqs 23 and 24 and physically corresponds to a freely jointed model in which all excluded-volume interactions are neglected except those between sites separated by two bonds. Although there is a net correlation hole over the range $1 < r < 6$, each of the curves shows a pronounced peak at contact and the weak shells of more distant neighbors. Clearly, as the local stiffness is increased, intramolecular screening is reduced and interior sites become much more susceptible to intermolecular contacts.

This trend is intensified in Figures 9 ($\xi_p = 2l$) and 10 ($\xi_p = 3l$), where, for clarity, the $N = 200$ results have been omitted. For these stiffer models, $g(r)$ appears relatively insensitive to chain length and exhibits a decaying oscillatory structure reminiscent of monatomic fluids. For a monatomic fluid at $\eta = 0.5$, the Percus–Yevick theory[22] predicts a contact value of $g(\sigma) = 5$ (as compared to the Carnahan–Starling prediction[30] of $g(\sigma) = 6$). As the chain length is increased from one though, intramolecular-screening and correlation-hole effects are quickly established, so that by $N = 20$, the local structure of these stiff chains is nearly identical with that of high polymers ($N = 2000$). This is consistent with MD results shown in Figures 4–6 and would seem to imply that, for stiff chains, the local effects of intramolecular screening are essentially independent of molecular weight. The largest difference between the two curves in Figure 10 appears at contact, though even here, $g(\sigma)$ decreases by only 8% as N varies over 2 orders of magnitude.

A second trend emerging from a comparison of Figures 7–10 is that as chain stiffness is increased, the local structure also becomes independent of ξ_p. Evidently, once enough stiffness has been introduced into the model to open the coils up and expose their interior sites, further straightening of the chains has little effect on local packing in the isotropic phase. To examine this further, we repeated the calculations for $N = 20$, 200, and 2000 and $\xi_p = 5$. At all r, the results were virtually indistinguishable from those shown in Figure 10.

Figure 11 shows the effect of varying the packing fraction at constant N and ξ_p. Results are for a 200-site chain at $\xi_p = 2l$ and η ranging from 0.1 to 0.4. At low densities $g(r)$ is dominated by self-screening effects, and a pronounced correlation hole is present, essentially devoid of significant structure. Under these conditions, where there is a relatively large amount of free volume, the reduction in configurational entropy required to bring two chains close enough together that they have a significant number of sites in close proximity is too great, and, on average, chains tend to remain apart, filling the available void spaces.[31] Cusps in the profiles can be identified at $r/\sigma = 2$ and stem from the use of rigid bonds in the model.[3,32] As the density is increased, chains are forced to pack closer together, leading to a steady evolution of short-range structure. By $\eta = 0.5$ (Figure 9) a site finds itself completely surrounded by neighboring sites and cannot easily distinguish between those that are members of the same

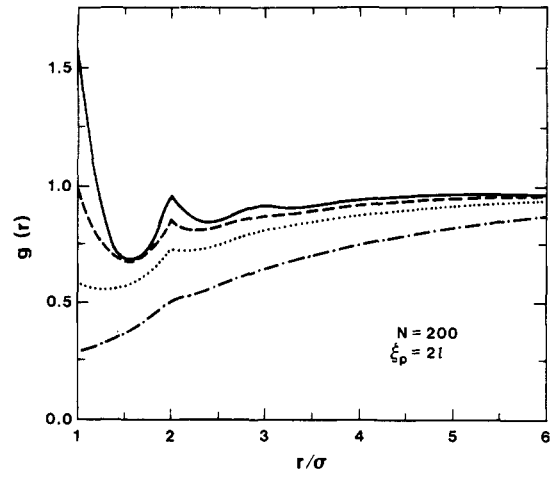

Figure 11. Packing-fraction dependence of the intermolecular radial distribution function. $N = 200$, $\xi_p = 2l$, and $\eta = 0.1$ (dash–dot), $\eta = 0.2$ (dot), $\eta = 0.3$ (dash), and $\eta = 0.4$ (solid).

chain and those that are not. Under these conditions, the local structure begins to resemble that of a simple monatomic fluid, exhibiting the familiar peak and valley pattern. This qualitative picture forms the underlying motivation for several mean-field equations of state for chains based on monatomic reference fluids.[33] However, a shallow, long-range correlation hole must still be present due to chain connectivity, excluded volume, and the near incompressibility of dense melts.[1-3,12]

The connection to thermodynamics is most readily made through the compressibility equation, which relates the isothermal compressibility, $\kappa_T = \rho_m^{-1}(\partial\rho_m/\partial P)_T$ to the total density fluctuations.[34] (Here, P denotes the pressure.) In terms of site–site correlation functions, the compressibility equation may be written[1,5,8]

$$\rho_m k_B T \kappa_T = \hat{\omega}(0) + \rho_m \hat{h}(0) \tag{35}$$

where the right-hand side of eq 35 will be recognized as the zero wave vector limit of the static structure factor. Substituting from the transformed, generalized Ornstein–Zernike equation (eq 3), this result becomes

$$\rho_m k_B T \kappa_T = \frac{N}{1 - \rho_m N \hat{c}(0)} \tag{36}$$

where we have used the identity $\hat{\omega}(0) = N$. In principle, eq 36 can be integrated over density, providing a straightforward route to the equation of state.[6]

In Figure 12, predictions for the isothermal compressibility at $\eta = 0.5$ are plotted in dimensionless form over a range of persistence lengths as a function of inverse chain length. The flexible-chain fluids exhibit a relatively large compressibility and N dependence. As the persistence length is increased, however, κ_T becomes much smaller and (like the radial distribution function) relatively insensitive to chain length or persistence length. This suggests that flexible Gaussian and freely jointed models will tend to overestimate κ_T, relative to real chains with excluded volume. This accounts, in part, for the anomalously low predictions for the pressure previously obtained from the compressibility equation for freely jointed chains.[6]

The drop in compressibility as stiffness is increased may be understood by noting that although the different fluids represented in Figure 12 are at the same packing fraction, they are not at the same pressure. For hard chains, the pressure is roughly proportional $g(\sigma)$.[6] Accordingly, the stiff-chain fluids are at much higher pressures than their flexible counterparts and, as such, would be

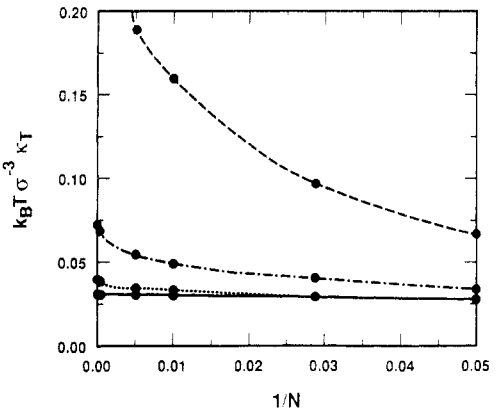

Figure 12. Dimensionless isothermal compressibility vs inverse chain length. Each curve is for a fixed persistence length: $\xi_p = l$ (dash), $\xi_p = 1.33l$ (dash–dot), $\xi_p = 2l$ (dot), and $\xi_p = 5l$ (solid). Note that as ξ_p increases, κ_T becomes relatively insensitive to chain length and stiffness. Points are polymer RISM results; curves are intended as a guide to the eye. (For $\xi_p = l$ and $N = 5000$, $k_BT\sigma^3\kappa_T \approx 0.338$.)

expected to be less compressible. This result is consistent with the intuitive physical argument that if the chains are imagined to be confined in a box subject to a small, virtual compression, the stiff chains will offer more internal resistance to the compression than will their flexible counterparts, which can more easily rearrange to accommodate the decrease in volume.

IV. Conclusions

Our aim in applying polymer RISM theory to semiflexible melts has been twofold: (i) to demonstrate the accuracy of the theory in describing real chain systems with excluded volume and (ii) to investigate the effects of chain stiffness and length on the local structure and isothermal compressibility. To this end, we developed a semiflexible model which is the discrete analogue of the continuous, wormlike chain. In this model, local stiffness is controlled by a single parameter, the persistence length, which, through a matching procedure, can be adjusted to reflect the local stiffness present in real chains due to molecular bonding constraints and torsional potentials, as well as induced stiffness arising from residual, unscreened excluded-volume interactions. The intramolecular structure factor is approximated by using the Koyama distribution, thus providing the required input into the RISM formalism. It is worth noting that the methods employed here are not limited to the SFC but, rather, can be applied to any model for which the second and fourth moments of the end-to-end probability distribution are known.

Comparison of the predicted intramolecular structure factors with the simulation results of Grest and Kremer indicates that the SFC model, in conjunction with the Koyama distribution, gives a much more accurate representation of intramolecular structure than either Gaussian or NFJC models, particularly in the intermediate scaling regime. Predictions for the intermolecular radial distribution function are found to be in excellent agreement with simulation results on all length scales, confirming the accuracy of polymer RISM theory when combined with a realistic model for intramolecular structure. These comparisons represent a rather stringent test in two respects: First, the bead–spring model used in the simulations had no inherent stiffness—all apparent stiffness was induced through unscreened, excluded-volume interactions which the SFC had to account for by an effective persistence length; and second, the relative flexibility of the simulated chains increased reliance on the approximate overlap correction described in section II.C. For chains with an inherent local stiffness imposed by bonding constraints and rotational potentials, both of these effects will be diminished. The calculations reported here, in conjunction with experimental and computational confirmation of the ideality theorem, suggest that, for dense melts, an accurate representation of intramolecular structure over a distance of two to three bond lengths is more important than a rigorous accounting of long-range excluded volume.

Parametric studies of the tangent hard-sphere model show a relatively large N dependence in $g(r)$ for flexible chains. However, as the persistence length is increased, both κ_T and the local structure saturate, becoming relatively insensitive to chain length and chain stiffness.

A promising feature of the SFC is that it appears amenable to a self-consistent treatment of the intramolecular and intermolecular correlations. In this study, the persistence length is determined by matching $\langle R^2 \rangle$ to simulation results. However, it would be desirable to develop a self-contained theory in which the persistence length is naturally determined through a self-consistent treatment of the intra- and intermolecular correlations. This is of particular interest in treating dilute solutions, flexible conjugated polymer liquids,[35] and polymer blends, where the ideality approximation might be expected to seriously break down. We have recently developed a theoretical framework which accounts for the coupling between intra- and intermolecular pair correlations and avoids the matching procedure used here. Numerical calculations along these lines are in progress.

Acknowledgment. We are very grateful to Dr. Gary Grest and Prof. Kurt Kremer for communicating several of their results prior to publication.

References and Notes

(1) Schweizer, K. S.; Curro, J. G. *Phys. Rev. Lett.* **1987**, *58*, 246. Curro, J. G.; Schweizer, K. S. *Macromolecules* **1987**, *20*, 1928.
(2) Curro, J. G.; Schweizer, K. S. *J. Chem. Phys.* **1987**, *87*, 1842.
(3) Schweizer, K. S.; Curro, J. G. *Macromolecules* **1988**, *21*, 3070.
(4) Curro, J. G.; Schweizer, K. S.; Grest, G. S.; Kremer, K. *J. Chem. Phys.* **1989**, *91*, 1357.
(5) Schweizer, K. S.; Curro, J. G. *Macromolecules* **1988**, *21*, 3082.
(6) Schweizer, K. S.; Curro, J. G. *J. Chem. Phys.* **1988**, *89*, 3342, 3350.
(7) Schweizer, K. S.; Curro, J. G. *Phys. Rev. Lett.* **1988**, *60*, 809. Curro, J. G.; Schweizer, K. S. *J. Chem. Phys.* **1988**, *88*, 7242. Schweizer, K. S.; Curro, J. G. *J. Chem. Phys.* **1989**, *91*, 5059. Curro, J. G.; Schweizer, K. S. *Macromolecules* **1990**, *23*, 1402.
(8) Chandler, D.; Andersen, H. C. *J. Chem. Phys.* **1972**, *57*, 1930. Chandler, D. *J. Chem. Phys.* **1973**, *59*, 2742. Chandler, D. In *Studies in Statistical Mechanics VIII*; Montroll, E. W., Lebowitz, J. L., Eds.; North-Holland: Amsterdam, 1982; pp 275–340.
(9) Chandler, D.; Pratt, L. R. *J. Chem. Phys.* **1976**, *65*, 2925. Pratt, L. R.; Chandler, D. *J. Chem. Phys.* **1977**, *66*, 147. Pratt, L. R.; Hsu, C. S.; Chandler, D. *J. Chem. Phys.* **1978**, *68*, 4202.
(10) Flory, P. J. *J. Chem. Phys.* **1949**, *17*, 303.
(11) Flory, P. J. *Principles of Polymer Chemistry*; Cornell University Press: Ithaca, NY, 1953; pp 425, 601–602.
(12) de Gennes, P.-G. *Scaling Concepts in Polymer Physics*; Cornell University Press: Ithaca, NY, 1979; pp 54–59.
(13) Ballard, D. G. H.; Wignall, G. D.; Schelten, J. *Eur. Polym. J.* **1973**, *9*, 965. Cotton, J. P.; Decker, D.; Benoit, H.; Farnous, B.; Higgins, J.; Jannink, G.; Ober, R.; Picot, C.; des Cloizeaux, J. *Macromolecules* **1974**, *7*, 863. Kirste, R. G.; Kruse, W. A.; Ibel, K. *Polymer* **1975**, *16*, 120. Flory, P. J. *Faraday Discuss. Chem. Soc.* **1979**, *68*, 14. Flory, P. J. *Pure Appl. Chem.* **1984**, *56*, 305.
(14) Curro, J. G. *J. Chem. Phys.* **1974**, *61*, 1203. Wall, F. T.; Seitz, W. A. *J. Chem. Phys.* **1977**, *67*, 3722. Curro, J. G. *Macromolecules* **1979**, *12*, 463. Kremer, K. *Macromolecules* **1983**, *16*, 1632. Theodorou, D. N.; Suter, U. W. *Macromolecules* **1985**,

18, 1467. Khalatur, P. G.; Papulov, Y. G.; Pavlov, A. S. *Mol. Phys.* **1986**, *58*, 887.
(15) Yamakawa, H. *Modern Theory of Polymer Solutions*; Harper and Row: New York, 1971; pp 52–57; *Pure Appl. Chem.* **1976**, *46*, 135; *Annu. Rev. Phys. Chem.* **1984**, *35*, 23.
(16) Freed, K. F. *Renormalization Group Theory of Macromolecules*; Wiley: New York, 1987; pp 28–33. Flory, P. J. *Statistical Mechanics of Chain Molecules*; Wiley: New York, 1969; pp 16, 401–403.
(17) Kratky, O.; Porod, G. *Recl. Trav. Chim.* **1949**, *68*, 1106.
(18) Koyama, R. *J. Phys. Soc. Jpn.* **1973**, *34*, 1029.
(19) Saito, N.; Takahashi, K.; Yunoki, Y. *J. Phys. Soc. Jpn.* **1967**, *22*, 219.
(20) Mansfield, M. L. *Macromolecules* **1986**, *19*, 854.
(21) Kremer, K.; Grest, G. S. *J. Chem. Phys.* **1990**, *92*, 5057. Also see: Grest, G. S.; Kremer, K. *Phys. Rev. A* **1986**, *33*, 3628; Kremer, K.; Grest, G. S.; Carmesin, I. *Phys. Rev. Lett.* **1988**, *61*, 566.
(22) Percus, J. K.; Yevick, G. J. *Phys. Rev.* **1958**, *110*, 1. Wertheim, M. S. *Phys. Rev. Lett.* **1963**, *10*, 321. Thiele, E. *J. Chem. Phys.* **1963**, *39*, 474.
(23) Lowden, L. J.; Chandler, D. *J. Chem. Phys.* **1973**, *59*, 6587.
(24) Porod, G. *J. Polym. Sci.* **1953**, *10*, 157.
(25) Andersen, H. C.; Weeks, J. D.; Chandler, D. *Phys. Rev. A* **1971**, *4*, 1597.
(26) Doi, M.; Edwards, S. F. *The Theory of Polymer Dynamics*; Clarendon: Oxford, 1986; p 23. Also see ref 12, p 36.
(27) Grest, G. S., private communication.
(28) Honnell, K. G.; Hall, C. K. In *Equations of State: Theories and Applications*; American Chemical Society: Washington, DC, 1986; pp 201–213. Also see ref 12, pp 62–65.
(29) Hansen, J. P. *Theory of Simple Liquids*; Academic: London, 1976; pp 119, 120. Gray, C. G.; Gubbins, K. E. *Theory of Molecular Fluids*; Clarendon: Oxford, 1984; Vol. I, pp 400–403. Streett, W. B.; Tildesley, D. J. *Faraday Discuss. Chem. Soc.* **1978**, *66*, 27. Labik, S.; Nezbeda, I. *Mol. Phys.* **1983**, *48*, 97. Streett, W. B.; Gubbins, K. E. *Annu. Rev. Phys. Chem.* **1977**, *28*, 373. Nezbeda, I.; Smith, W. R. *Chem. Phys. Lett.* **1981**, *81*, 79. Chandler, D.; Hsu, C. S.; Streett, W. B. *J. Chem. Phys.* **1977**, *66*, 5231.
(30) Carnahan, N. F.; Starling, K. E. *J. Chem. Phys.* **1969**, *51*, 635.
(31) See ref 11, pp 519–530.
(32) Ladanyi, B. M.; Chandler, D. *J. Chem. Phys.* **1975**, *62*, 4308.
(33) Croxton, C. A. *Phys. Lett. A* **1979**, *70*, 441. Dickman, R.; Hall, C. K. *J. Chem. Phys.* **1986**, *85*, 4108. Honnell, K. G.; Hall, C. K. *J. Chem. Phys.* **1989**, *90*, 1841.
(34) McQuarrie, D. A. *Statistical Mechanics*; Harper and Row: New York, 1976; pp 268, 269.
(35) Schweizer, K. S. *J. Chem. Phys.* **1986**, *85*, 1156, 1176. Schweizer, K. S. *Synth. Met.* **1989**, *28*, C565.

Phase Behavior of Sulfur-Containing Polymers: Polythioesters

C. Berti,* E. Marianucci, and F. Pilati

Dipartimento di Chimica Applicata e Scienza dei Materiali, Università di Bologna, Viale Risorgimento 2, 40136 Bologna, Italy

A. Roviello and A. Sirigu*

Dipartimento di Chimica, Università di Napoli, Via Mezzocannone 4, 80134 Napoli, Italy

Received October 2, 1989; Revised Manuscript Received December 11, 1989

ABSTRACT: Three polythioesters containing the 4,4′-dithiobiphenyl group have been synthesized by reaction under interfacial conditions of 4,4′-dimercaptobiphenyl with 1,5-pentanedicarbonyl dichloride (polymer P5), 1,10-decanedicarbonyl dichloride (polymer P10), or 1,13-tridecanedicarbonyl dichloride (polymer P13). They were characterized by FT-IR, ^{1}H NMR, and GPC methods, and their phase behavior was investigated by DSC, polarizing microscopy, and X-ray diffraction techniques. The DSC heating curve of each polymer shows two endothermic signals that are almost coalescent in the case of P13, indicating that the second phase transition occurs in addition to melting. The X-ray diffraction evidence suggests that for polymers P5 and P10 the first phase transition is a solid–solid one. These polymers melt to an isotropic liquid. Some birefringence may reversibly be induced by mechanical shear of this phase whose X-ray diffraction pattern is typical of an amorphous structure. The first phase transition observed for P13 is the melting. An optically anisotropic liquid is produced whose morphological features are indicative of a nematic liquid crystal. This phase has a narrow thermal stability range. Possible effects of molecular weight on the phase behavior are not taken into account; they could play some role in the case of P10.

Introduction

The liquid crystal properties of some polyalkanoates of 4,4′-dihydroxybiphenyl have been investigated by several authors[1,2] and particularly by Krigbaum et al.[3,4] Their nematogenic or smectogenic character, depending on the odd or even number of methylene groups contained in the flexible spacer, has been discussed.

This article reports the results of an investigation of the phase behavior of three polythioesters containing 4,4′-dithiobiphenyl groups. Some results of an investigation on the possible consequences of replacing with sulfur atoms oxygen atoms of ester groups are available for some low molecular weight mesogenic thiobenzoates[5–7] or for several cholesteric mesogens such as 3β-(*n*-alkanoylthio)-5α-cholestene[8] or 3β-((*ω*-phenylalkanoyl)thio)-5α-cholestene;[8–11] in addition, the effect of the substitution has been discussed for polymeric liquid crystals containing ether or thioether groups.[12] As a general trend, sulfur-containing compounds have higher mesophase stability than the oxygenated homologues.

Results and Discussion

Polythioesters were obtained by reacting 4,4′-dimercaptobiphenyl (DMB) with aliphatic acid dichlorides under interfacial conditions in the presence of benzyltriethylammonium chloride (BTEAC) as the catalyst,

0024-9297/90/2223-3505$02.50/0